

Deliverable D1.4

Devices for mechanical characterisation at laboratory scale that are operational

Document type	Deliverable D 1.4
Document Version / Status	2.5
Primary Authors	Dietmar Gruber, dietmar.gruber@unileoben.ac.at, MUL
Distribution Level	PU (Public)
Project Acronym	ATHOR
Project Title	Advanced THERmomechanical multiscale mOdelling of Refractory linings
Grant Agreement Number	764987
Project Website	www.etn-athor.eu
Project Coordinator	Marc Huger, marc.huger@unilim.fr, UNILIM Dietmar Gruber, dietmar.gruber@unileoben.ac.at, MUL Marc Huger, marc.huger@unilim.fr, UNILIM Eric Blond, eric.blond@univ-orleans.fr, UORL Hung Thanh Nguyen, thanh.nguyen@unileoben.ac.at, MUL Soheil Samadi, soheil.samadi@unileoben.ac.at, MUL
Document Contributors	Lucas Teixeira, lucas.breder-teixeira@univ-orleans.fr, UORL Farid Asadi, farid.asadi@unilim.fr, UNLIM Robert Kaczmarek, robert.kaczmarek@unilim.fr, UNLIM Ilona Kieliba, kieliba@ghi.rwth-aachen.de Vahid Tadaion, tadaion@ghi.rwth-aachen.de Thorsten Tonnesen, tonnesen@ghi.rwth-aachen.de

Change log

Version	Date	Change	Page
1.0	05.12.2018	Creation of the first version	all
2.0	21.12.2018	Inclusion of the table	2-6
2.1	31.12.2018	Type setting and introduction	all
2.2	18.02.2019	Inclusion of section 4	8-32
2.3	03.05.2019	Proof reading	all
2.4	06.05.2019	Reformatting	all
2.5	08.05.2019	Proof reading	all

Table of contents

1. INTRODUCTION	3
2. LIST OF DEVICES	3
3. TABLE SUMMARIZING THE MOST IMPORTANT INFORMATION.....	4
4. SOME DETAILS ABOUT EXPERIMENTAL DEVICES	7
4.1. Ultrasonic device for elastic properties measurements at room temperature	7
4.2. Ultrasonic device for elastic properties measurements at high temperature under a controlled atmosphere	8
4.3. Acoustic emission device for monitoring damage at high temperature under controlled atmosphere	9
4.4. Wedge Splitting test at room temperature combined with 2 Parts Digital Image Correlation.....	9
4.5. Mechanical device for the tensile (compression) test at high temperature under a controlled atmosphere	11
4.6. Diametrical compression test (Brazilian test) at high temperature in a controlled atmosphere combined with Digital Image Correlation (DIC)	11
4.7. Wedge splitting test at room temperature and elevated temperature	13
4.8. Mini wedge splitting test device at room temperature	15
4.9. Uniaxial tensile creep test device.....	18
4.10. Uniaxial compressive creep test device	20
4.11. RFDA - Resonant Frequency and Damping Analyser	23
4.12. Diametrical compression test (Brazilian test) at room temperature combined with Digital Image Correlation	24
4.13. DEBEN device for "in situ" room temperature micromechanical test.....	26
4.14. Cyclic Thermal Shock Test - The Twin-chamber equipment	27
5. REFERENCES	29

1. Introduction

The ATHOR project is dedicated to the development of experimental and computational methods to characterize and model refractory materials. This requires mechanical material characterisation to determine material parameters and to verify simulation results. It is very important to characterise material properties at room temperature and at application temperatures as well because the material behaviour differs significantly.

The characterisation includes methods for the determination of the Young's modulus and Poisson ratio, the fracture mechanical behaviour and the creep behaviour.

Young's modulus and Poisson ratio define the linear elastic material behaviour. Due to the fact that in refractories material failure can not be avoided, the characterisation of the fracture mechanical behaviour and the creep behaviour is essential for the understanding of the material behaviour and for further improvement of refractories and linings.

In this report for the task 1.4 "Devices for thermomechanical characterization", a list of available devices for the characterisation of the thermomechanical behaviour and their uses in the ATHOR network is given in section 2. For some tests (wedge splitting test, Brazilian test, Young's modulus testing), devices with different characteristics are available. The table in section 3 summarizes the most important information concerning the devices and a detailed description of each device is provided in section 4.

2. List of devices

1. Ultrasonic device for elastic properties measurement at room temperature (IRCER - UNILIM)
2. Ultrasonic device for elastic properties measurement at high temperature in controlled atmosphere (IRCER - UNILIM)
3. Acoustic emission device for damage monitoring at high temperature in controlled atmosphere (IRCER - UNILIM)
4. Wedge Splitting test at room temperature combined with 2 Parts Digital Image Correlation (IRCER - UNILIM)
5. Tensile test under controlled atmosphere at room temperature and elevated temperatures (IRCER - UNILIM)
6. Diametrical compression test (Brazil test) at high temperature in controlled atmosphere combined with Digital Image Correlation (LaMé - UORL)
7. Wedge splitting test at room temperature and elevated temperature (CoC - MUL)
8. Mini wedge splitting test at room temperature (CoC - MUL)
9. Creep under tensile loads (CoC - MUL)
10. Creep under compressive loads (CoC - MUL)
11. RFDA - Resonant Frequency and Damping Analyser (RWTH and CoC - MUL)
12. Diametrical compression test (Brazil test) at room temperature combined with Digital Image Correlation (IRCER - UNILIM)
13. DEBEN device for "in situ" room temperature micromechanical test (miniaturized bending test, miniaturized wedge splitting test) combined with Digital Image Correlation (DIC) (IRCER - UNILIM)
14. Cyclic Thermal Shock Test - The Twin-chamber equipment (GHI - RWTH)

3. Table summarizing the most important information

Nr.	Purpose	Sample geometry	Application temperature	Atmosphere	Main interest	Disadvantage
1	Elastic properties with sound velocity method. Different modes (transversal or longitudinal and transmission or reflection) are possible.	Plate with two parallel faces. Dimensions: thickness (of few mm to few cm) depends on the signal damping and of the biggest grain size. The bigger the grain size is, the thicker the sample should be to obtain representative results.	Room temperature	Air	Young's modulus, shear modulus and Poisson's ratio determination. Evaluation of anisotropy	If the sample strongly attenuates ultrasonic waves, a measurement of thicker samples becomes impossible. If the microstructure contains big grains, the measurement is possibly not representative.
2	Elastic properties with sound velocity method	Cuboid. Dimensions: height from 60 to 150 mm and base side from 5 to 13 mm. Dimensions depend on the waveguide (e.g. diameter), ultrasonic waves frequency, and material properties (including stiffness and density). Sample dimensions are adjusted using a special simulator.	25-1750°C	Air, argon	Young's modulus evolution during thermal cycling in a specific atmosphere	In contrary to RFDA, the sample needs to be glued using special cement. In case of erroneous cement preparation, the results could represent not only the changes of the sample, but also of the cement.
3	Acoustic emissions due to microstructural changes during thermal treatment are detected (e.g. cracks formation)	Cuboid : Dimensions: height of 25 mm and base side of 5 mm	25-1550°C	Air, argon	Information about temperature range and stage of a thermal cycle at which different damage within the microstructure could be generated.	False acoustic emissions in case of incorrect equipment calibration (e.g. too low signal's amplitude threshold) or sample movements during experiment.
4	Wedge splitting test allows stable fracture mechanical tests on quasi-brittle materials. For this reason, special load transmission pieces (composed of wedge, two rolls and two load transmission pieces) are used to transfer the vertical load, applied with a uniaxial testing machine, to a horizontal one, causing a very stable crack opening. Sample fracture propagates from the starting notch in the direction of the linear support.	Cubic sample with groove (for loading device) and starting notch. Dimensions: side of a cube of 100 mm; groove with dimensions of 22.5x22.5x100 mm ³ ; starter notch with dimensions of 3.5x12.5x100 mm ³	Room temperature	Air	Observation of crack propagation using 2P-DIC (Two parts digital image correlation) Analysis of load-displacement curve (using standard DIC). Determination of fracture energy.	Sample shape can be too small for the development of the full fracture process zone, especially in case of refractories with reduced brittleness.

5	The purpose of the tensile test is to obtain stress-strain characteristics of tested material at a given temperature. It's possible test both in tension or compression and using one or more testing cycles (allows observation of gradual sample degradation).	Cylindrical rod Dimensions: sample length of 170 mm and diameter of 20 mm; reduced section length of about 30 mm (to place the extensometers with the gauge length of 25 mm) and diameter of 16 mm;	25-1600°C	Air, argon	Young's modulus at given temperature derived from the initial part of the stress-strain curve. Observation of material's behaviour - linear or non-linear - closely linked with phenomena occurring in tested materials.	Long procedure of sample preparation, drying, gluing to the sample holders, uniaxial machining, sample holders isolating for high temperature tests Complex calibration of extensometers
6	The purpose of the diametric compression test is to perform the identification of material's parameters considering different constitutive laws, such as for example elastic and viscoplastic ones.	The use of I-DIC doesn't require any standardized sample's size. For standard materials, a sample with 50mm diameter and 50mm thickness will be used	Furnace 1: 25-1250°C; Furnace 2: 25-1500°C	Furnace 1: Air, argon; Furnace 2: Air	Identification of nonlinear behaviour of materials for further use in numerical simulations.	The identification requires a priori assumption about the constitutive behaviour of the material, which is normally not known. The temperature range of Furnace 1, which has the possibility of using a reducing atmosphere, is too low. The use of optical devices at high temperatures is complex.
7	Wedge splitting test for fracture testing of refractories.	Geometry: cubic sample with groove (for load transmission pieces) and starting notch. Dimensions: side of a cube of 100x100x70 mm ³ . Groove with dimensions of 22.5x22.5x100 mm ³ . Notch with dimensions of 3.5x12.5x100 mm ³ .	25-1500°C	Air, argon	Observation of the fracture mechanism of refractory materials, determination of the specific fracture energy, nominal notch tensile strength and strain softening behaviour via inverse evaluation	Impossible to observe the crack propagation in the SEM because of geometrical considerations Results from high temperature measurements may be influenced by creep
8	Mini wedge splitting test for the identification the fracture mechanism of refractory material on a microscale level	Geometry: cubic sample with notch. Dimensions: side of a cube of 25x21x8 mm ³ . Notch with dimensions of 10x1x8 mm ³ .	Room temperature	Air	Direct observation of the fracture behaviour of refractory material under light microscope and SEM	Only observation of crack initiation is possible because the sample is small
9	Identification of uniaxial tensile creep	Cylinder: 230mmx30mm(diameter)	Up to 1500°C	Air/coke breeze	Observation of strain-time creep curve and identification of creep parameters with regard to a creep law.	Measurement is only possible in one direction. Measurement using corundum extensometers introduce some errors.
10	Identification of uniaxial compressive creep	Cylinder: 70mmx35mm(diameter)	Up to 1500°C	Air/coke breeze	Observation of strain-time creep curve and identification of creep parameters with regard to a creep law.	Measurement is only possible in one direction. Measurement using corundum extensometers introduce some errors.

11	Elastic properties Young's modulus, shear modulus and Poisson's ratio determination	Rectangular or circular in cross section	25-1500°C	Air	In-situ characterization and monitoring of thermally induced microstructural processes e.g. phase transition, viscous phase formation, damage or fatigue. With modified sample geometry, also in-situ monitoring of corrosion processes is possible.	Sensitive to dimensional tolerances. Big scattering of data at high temperature possible depending on the type of material and damage state. Especially in case of damping measurements, there is a lack of fundamental knowledge relating to microstructural phenomena with the damping behaviour of ceramic materials. This causes difficulties in results interpretation.
12	Brazilian test to compare and investigate the tensile strength of the materials	Geometry: cylinder Dimensions: diameter of 50 mm and thickness from 10 to 50 mm	Room temperature	Air	To compare and investigate the tensile strength of the materials. It is an indicator for the strength of the materials	Difficulties to assure correct load distribution Tensile, compressive and shear loads occur simultaneously in one sample
13	Investigating the initiation of microcracks affected by microstructures under bending or splitting loads Use of the digital image correlation method to obtain the strain fields evolution.	Mini wedge splitting, Micro bending test: Geometry: rectangular parallelepiped Dimensions: different, for example: 55x10x3 mm used in Limoges for bending up to now.	Room temperature	Air	To obtain strain field of materials, investigating the initiation of microcracks affected by microstructures of the material. This test is especially interesting for the small-scale analysis, as it can be performed under an optical microscope or in a scanning electron microscope (SEM).	Performing DIC under SEM or optical microscope needs special tools Fracture mechanical parameters are influence by the small fracture process zone.
14	Cyclic thermal shock test – a full cycle consists of one cold shock and one hot shock between two custom temperatures.	No specific geometry requirement. The specimen's dimensions should not exceed the sliding gate opening (max 200x150x60 mm ³ length, width and height respectively).	Max temperature 1500°C Max temperature gradient 900°C	Air	To impose cyclic thermal shock on a refractory specimen in an unconstrained condition between two elevated temperatures in a close system	No possibility to test carbon containing materials, which require a reducing environment for testing. No possibility to realise high-cycle fatigue tests. High maintenance equipment due to harsh testing conditions.

4. Some details about experimental devices

4.1. Ultrasonic device for elastic properties measurements at room temperature

This ultrasonic measurement device allows the determination of the Young's modulus E , shear modulus G and Poisson ratio of the investigated material [1], [2]. The device is composed of:

- Generator (power supply for transducers);
- Transducers (for measurement in longitudinal or transversal modes) working as emitter or receiver of ultrasonic waves;
- Attenuator and preamplifier;
- Oscilloscope used for digitalization of the useful part of ultrasonic signal (for further measurement of the flight time $\Delta\tau$ within sample thanks to further numerical treatment on computer);

The ultrasonic transducer is placed in direct contact with one surface of the test specimen and the sound waves are emitted directly onto its surface. The sound waves pass through the sample and are then either detected directly by a receiver or reflected back to the Emitter/Receiver. The strength of the measured signal depends on the selected frequency and the choice of either the transmission or reflection method (see Figure 1). Attenuation of the signal depends on intrinsic material properties, as well as specimen thickness. Specimen thickness is in the range of several mm to several cm.

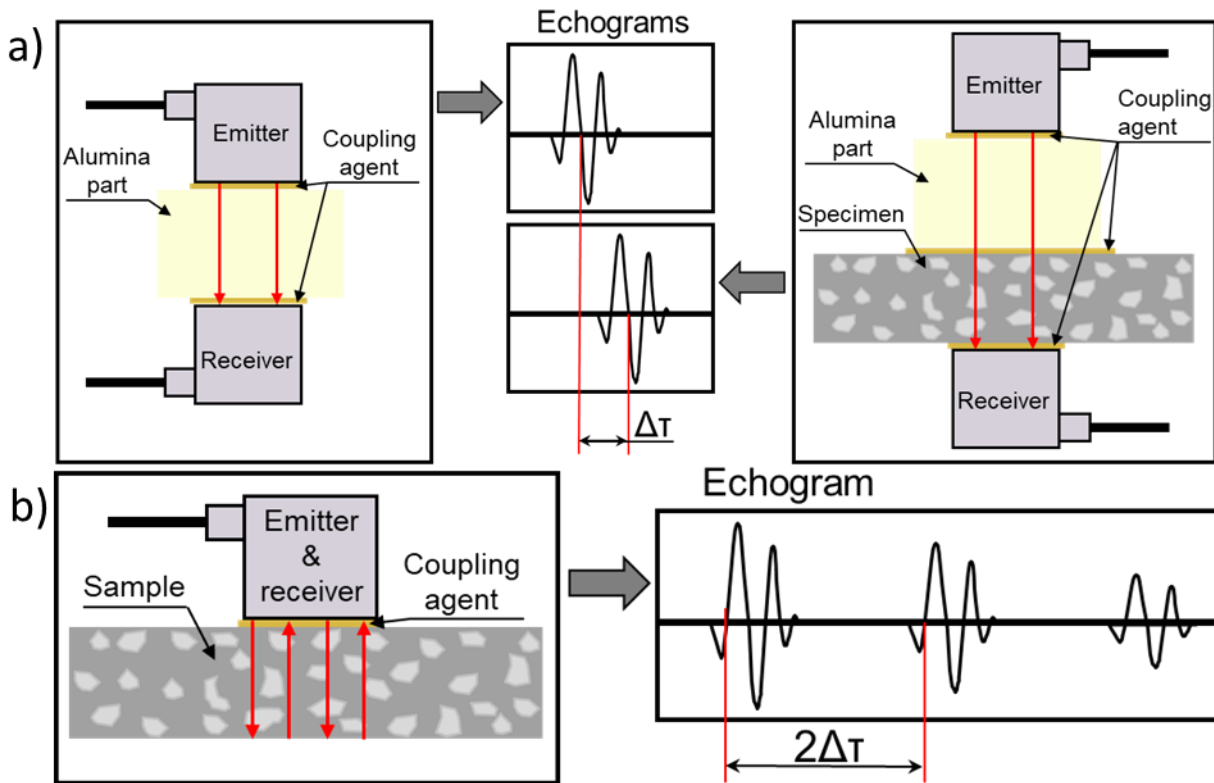


Figure 1: Experimental measuring device in infinite medium by a) transmission; b) reflection from N. Tessier-Doyen [1].

This method assumes the investigation of an infinite medium, having much greater dimensions, than the wavelength used. Two modes of ultrasonic measurement are used: longitudinal and transversal. Measurement in each mode allows the determination of longitudinal V_L and transversal V_T velocities, using equations from Table 1.

Table 1: Formulas for calculation of velocities in different modes.

	Transmission mode	Reflection mode
Longitudinal velocity	$V_L = \frac{e}{\Delta\tau_L}$	$V_L = \frac{2 \cdot e}{\Delta\tau_T}$
Transversal velocity	$V_T = \frac{e}{\Delta\tau_L}$	$V_T = \frac{2 \cdot e}{\Delta\tau_T}$

Once the V_L and V_T velocities are calculated and material's density is known, it is possible to calculate the aforementioned elastic properties, using the following equations (Equ. 1, Equ. 2, Equ. 3):

$$E = \rho \frac{3 * V_L^2 - 4 * V_T^2}{\frac{V_L^2}{V_T^2} - 1} \quad \text{Equ. 1}$$

$$G = \rho * V_T^2 \quad \text{Equ. 2}$$

$$\vartheta = \frac{E}{2G} - 1 \quad \text{Equ. 3}$$

4.2. Ultrasonic device for elastic properties measurements at high temperature under a controlled atmosphere

This ultrasonic device allows determination of the Young's modulus evolution during a thermal cycle. The device consists of (see Figure 2a):

- Transducer (composed of a magnetostrictive rod surrounded by a copper coil);
- Alumina waveguide glued to the magnetostrictive rod in order to transmit ultrasonic waves between the transducer and specimen.
- Specimen glued to the waveguide using a high alumina content adhesive;
- Furnace with high-temperature limit of 1750°C;

The transducer generates ultrasonic waves at a frequency inversely proportional to the length of the magnetostrictive rod. The ultrasonic waves then propagate through the alumina waveguide and specimen. Some of ultrasonic waves are reflected due to interface between the waveguide and specimen and others from the end of specimen (possible multi-reflections). An ultrasonic echogram is created from the ultrasonic waves that are reflected back to the transducer.

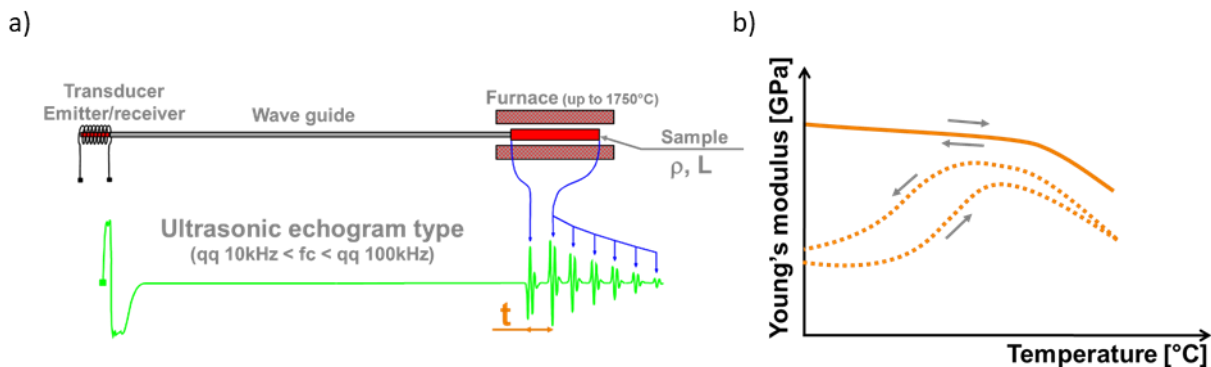


Figure 2: Elastic properties measurement at high temperature from R. Grasset-Bourdel [3]. a) Schematic of the device, b) Example of results for materials damaged and not damaged during thermal cycle.

The Young's modulus (E_{us}) can be calculated, as a function of specimen density and velocity of ultrasonic wave within the specimen, using Equ. 4:

$$E_{us} = \rho \cdot V^2 = \rho \cdot \left(\frac{2L}{\tau}\right)^2 \quad \text{Equ. 4}$$

where ρ is the material density, V is velocity of ultrasonic waves within specimen, L is specimen length and τ propagation time within specimen.

An example of results from two materials with different behaviours during thermal treatment is shown in Figure 2b. The curve with reversible behaviour indicates a stable material during heating while that with a hysteresis loop corresponds to a thermally damaged material.

4.3. Acoustic emission device for monitoring damage at high temperature under controlled atmosphere

This acoustic emission device is used for monitoring specimen damage during thermal cycles and consists of (see Figure 3a):

- Transducer Micro80 (from Physical Acoustic) working in the 200-900 kHz range;
- Alumina waveguide providing a good ultrasonic transmission between the specimen and transducer. The top end of this guide is carefully sharpened in order to optimised ultrasonic transmission from the specimen without any usage of cement (dry contact);
- Other specific alumina parts are used around the sample in order to guaranty a constant contact pressure between sample and wave guide (a constant transfer function is required during the entire test);
- Furnace with high-temperature limit of 1550°C.

This technique is based on recording of acoustic waves that correspond to sudden energy release phenomena, such as microcracking. Once a microcrack forms, the generated acoustic wave, within specimen, propagates through the waveguide to the transducer. All detected signals during the entire test are analysed using the Noesis software. Typical results of materials, involving damage during a thermal cycle, is presented in Figure 3b. Damage mainly occurs during cooling stage.

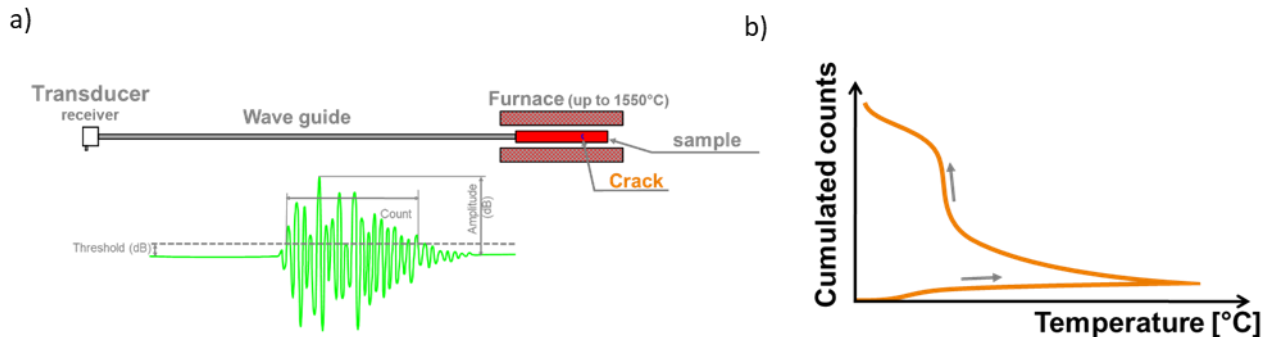


Figure 3: Acoustic emission device. a) Simplified schema of device with selected features of acoustic emission signal; b) Evolution of cumulated counts vs. temperature for a material which is partially damaged during thermal cycle. From R. Grasset-Bourdel [3].

4.4. Wedge Splitting test at room temperature combined with 2 Parts Digital Image Correlation

This wedge splitting test is used to analyse stable crack propagation within heterogeneous refractory materials as well as to evaluate mechanical properties such as specific fracture energy or nominal notch tensile strength.

The standard wedge splitting test setup (see Figure 4a) uses:

- Cubic specimen (100x100x100 mm³) with groove (24x22.5x100 mm³) and starting notch (3.4x12x100 mm³). Some details are indicate in Figure 5;
- Wedge, rolls, load transmission pieces to transfer the vertical load (applied by the testing machine) to a horizontal load (applied to the specimen);
- Linear support in contact with the bottom face of the specimen;
- CMOS camera to acquire images for optical measurements;
- LED lighting to keep stable lighting conditions during measurement;
- Classical DIC software to calculate the horizontal displacement δ_H between right and left specimen parts;
- 2P-DIC (two parts digital image correlation) software to obtain a digital representation of the cracks.

Universal testing machine applies a vertical load to the wedge, which is then transferred through rolls and load transmission pieces to the specimen (the load applied to the specimen has horizontal direction). The specimen is subjected to mode I crack opening. During measurement, CMOS camera acquires images, which are later used for analysis using digital image correlation techniques [4].

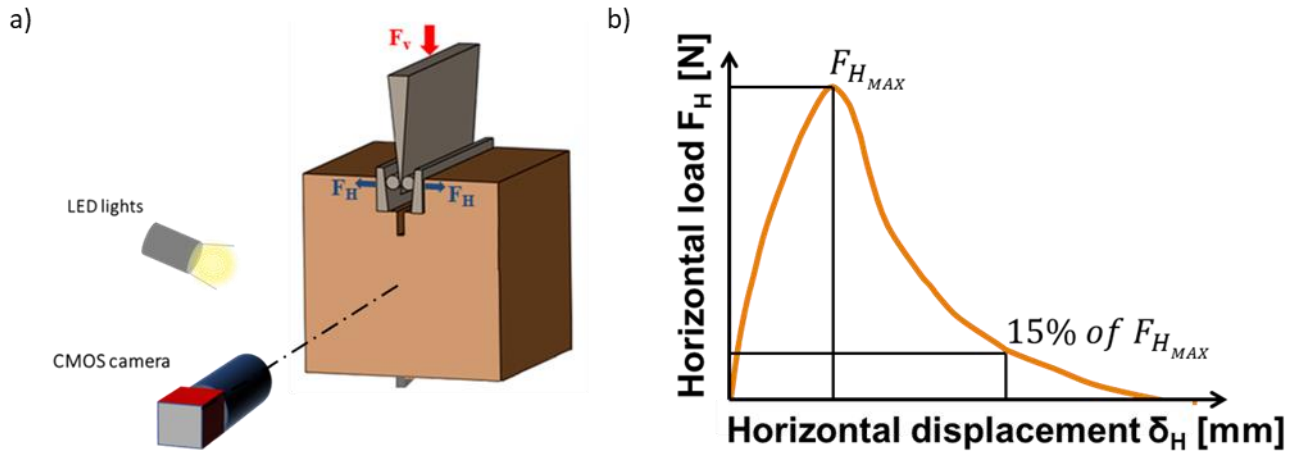


Figure 4: The wedge splitting test. a) Schema of the mechanical device with an image acquisition setup. From Y. Belrhiti [4],
b) A load displacement curve for quasi-brittle material.

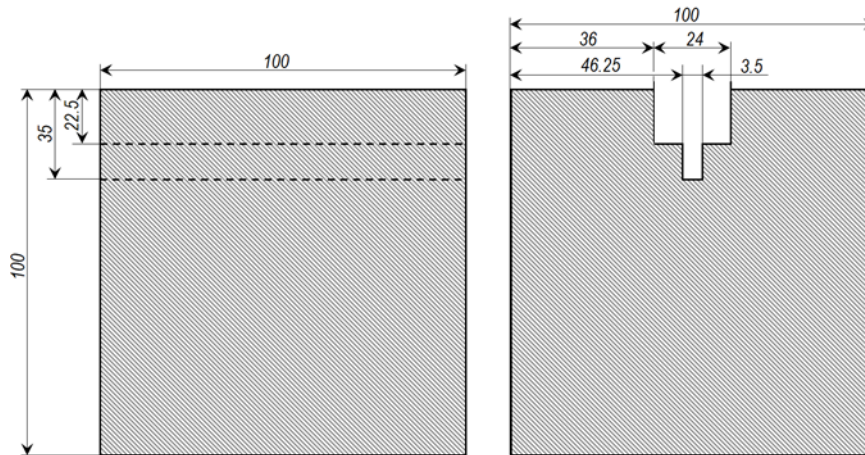


Figure 5: Sample dimensions for wedge splitting test.

A load-displacement curve (see Figure 4b) is plotted using values of:

- The horizontal load applied to the specimen (calculated from vertical load applied by the machine);
- The horizontal displacement δ_H between right and left specimen parts determined by DIC technique.

The material strength can be characterized using the nominal notch tensile strength parameter, which is determined using Equ. 5:

$$\sigma_{NT} = \frac{F_{H \max}}{b \cdot h} + \frac{6F_{H \max} \cdot y}{b \cdot h^2} \quad \text{Equ. 5}$$

where b and h are specimen dimensions, $F_{H \max}$ is maximum horizontal load and y is distance between F_H and the middle of h (h being the distance between the starter notch and the bottom of the specimen). The specific fracture energy G_f' , corresponding to the mean work per unit of projected fracture area required to propagate the crack, can be calculated using the Equ. 6:

$$G_f' = \frac{1}{A} \int_0^{\delta_{15\% F_{\max}}} F_H \cdot d\delta \quad \text{Equ. 6}$$

where A is fracture surface; F_H is horizontal load, and $\delta_{15\% F_{\max}}$ is δ_H corresponding to 15% of the maximal horizontal load.

4.5. Mechanical device for the tensile (compression) test at high temperature under a controlled atmosphere

This mechanical device for the tensile (compression) test is designed to investigate the stress-strain behaviour of materials at high temperature under a controlled atmosphere.

This device is composed of (see Figure 6a):

- Instron 8862 machine with:
 - rigid frame (100 kN)
 - two hydraulic grips, being well aligned with axis of machine (frequent aligning required);
 - a load cell with a maximum capacity of 5 kN;
- Specimen glued to metallic bushings, using a magnesium oxide based ceramic adhesive. Metallic bushings being then clamped by hydraulic grips;
- Two capacitive extensometers with SiC rods located on the opposite sides of the central part of specimen with a reduced diameter;
- Induction furnace with two susceptors: MoSi₂ (under air atmosphere) and graphite (under argon atmosphere). The temperature limit of this furnace is 1600°C.

The targeted load is applied to the specimen through the hydraulic grips. However, tests are mainly performed under displacement control (typical speed of 0.001 mm/s) using displacement actuator sensor. During the entire test, strain in the central part of the specimen is monitored by the 2 extensometers.

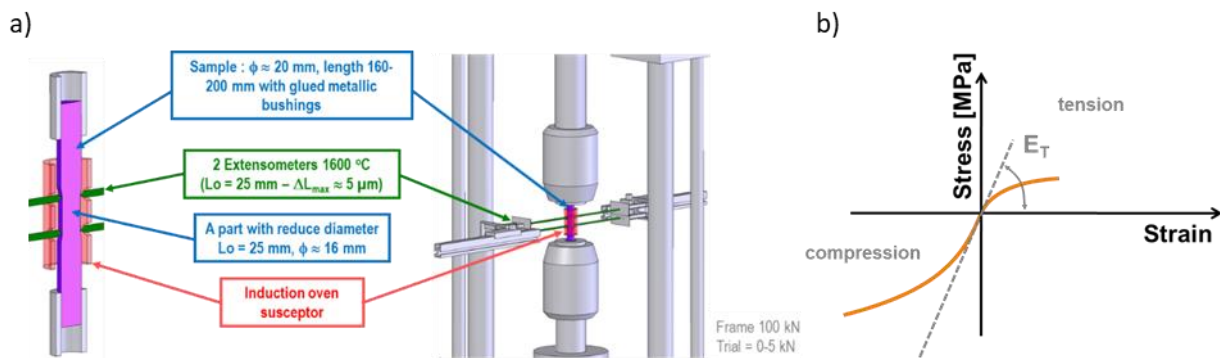


Figure 6: The tensile (compression) test. a) A 3D model of the mechanical device in tension with a description of selected components (From R. Grasset-Bourdel [3]); b) A stress-strain curve exhibiting non-symmetrical mechanical behaviour.

The very beginning of the stress-strain curve (rather elastic linear) is used to determine the Young's modulus by linear regression (typically between 0 and 0.5 MPa). Stress-strain curve of quasi-brittle materials can exhibit post-peak behaviour corresponding to energy dissipation phenomena. In refractory materials, non-symmetrical mechanical behaviour can be observed between tension and compression (see Figure 6b).

4.6. Diametrical compression test (Brazilian test) at high temperature in a controlled atmosphere combined with Digital Image Correlation (DIC)

This diametrical compression at high temperature in a controlled atmosphere combined with Digital Image Correlation (DIC) device, allows the inverse identification of materials parameters in tension and compression. The device will be employed for the inverse identification of creep parameters for different constitutive models at high temperature. Table 2 and Figure 7 show the equipment involved in this diametrical compression test.

Table 2: Equipment involved in the diametrical compression test

Part	Description
Furnace and testing machine	A standard testing machine is used to perform the tests. The furnace has a glass window, from which the sample can be seen and photographed during the test
CCD camera	Used to take the pictures during the test, that will be further analysed using a DIC software
LabVIEW software	A LabVIEW application is used to control the photos' parameters. It also synchronizes the beginning of the test with the beginning of photos' acquisition

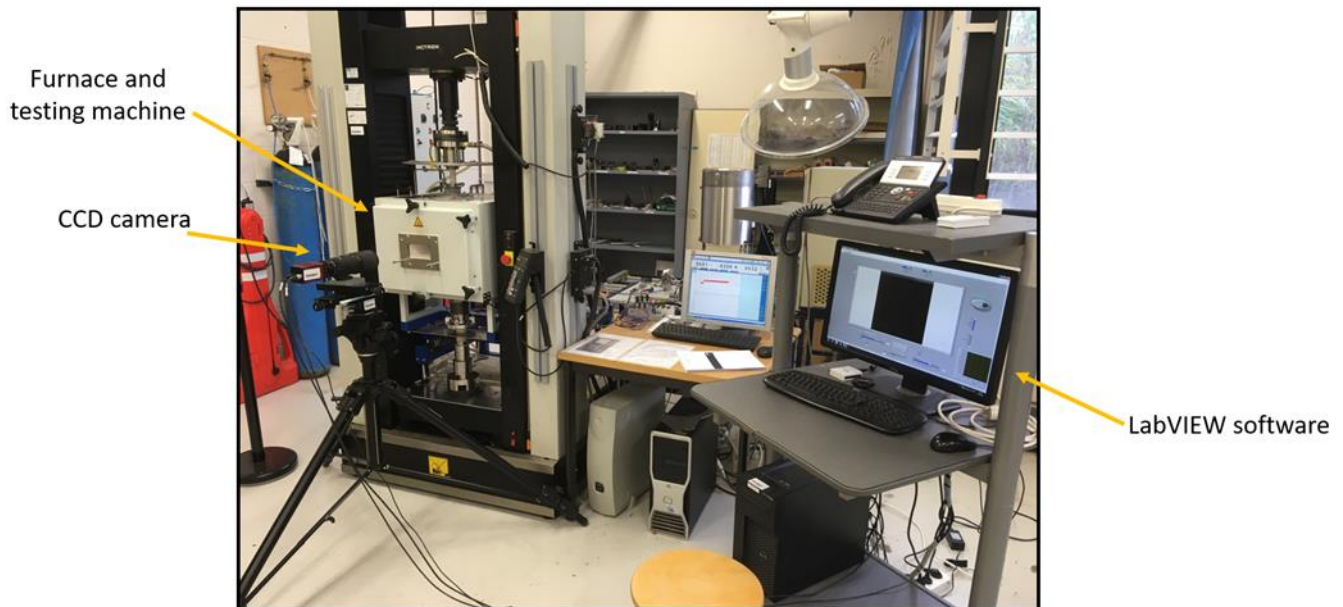


Figure 7: Equipment involved in the diametrical compression test.

Since the inverse identification of material parameters will make use of Digital Image Correlation techniques, no specific standard is required for the diametrical compression test. Nevertheless, it's suggested that the minimum dimension of the cylindrical sample be at least ten times higher than the maximum material's grain size, to guarantee the reproducibility of the tests.

The test's protocol, adopted at the University of Orléans, uses the Integrated Digital Image Correlation technique (I-DIC) [5]. In this technique, once the pictures from the diametrical compression test are obtained, a numerical model of the test is recreated in a Finite Element's program. The algorithm to obtain the material's parameters is (see Figure 8):

- Step 1: Define an initial guess for the values of the material's properties
- Step 2: Perform a numerical simulation of the test, using the material's properties previously defined
- Step 3: Apply the displacements' field obtained through the numerical simulation to the reference image (image obtained before the sample starts to be deformed). This is done by interpolating the pixels' grey levels' values.
- Step 4: Calculate the difference in the distribution of pixels' grey levels from the deformed experimental image and the theoretically deformed image
- Step 5: Check if the difference between the images is below a defined tolerance.
- Step 6: If the difference between the theoretically deformed image and the experimentally deformed image is above the tolerance, the initial guess for the material's properties is not correct. Therefore, an optimization algorithm needs to be used to define a new guess, and the computation returns to Step 2.

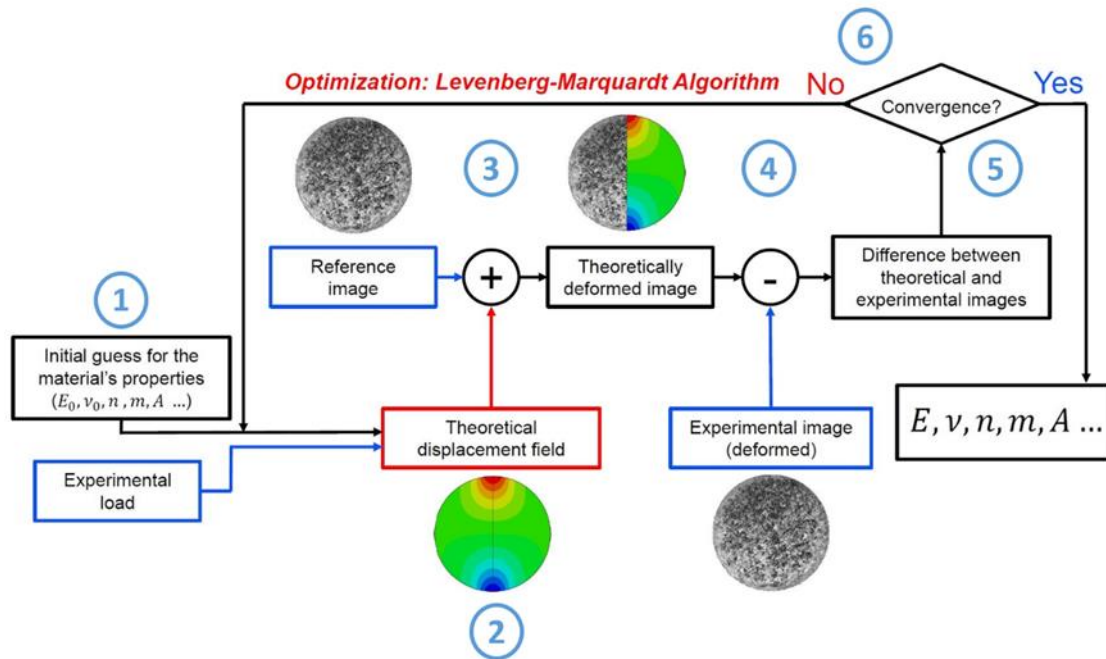


Figure 8: I-DIC algorithm.

Once the I-DIC algorithm converges, the material's parameters are obtained. Figure 9 shows an example of output from the I-DIC algorithm for the identification of the Young's modulus of a material.

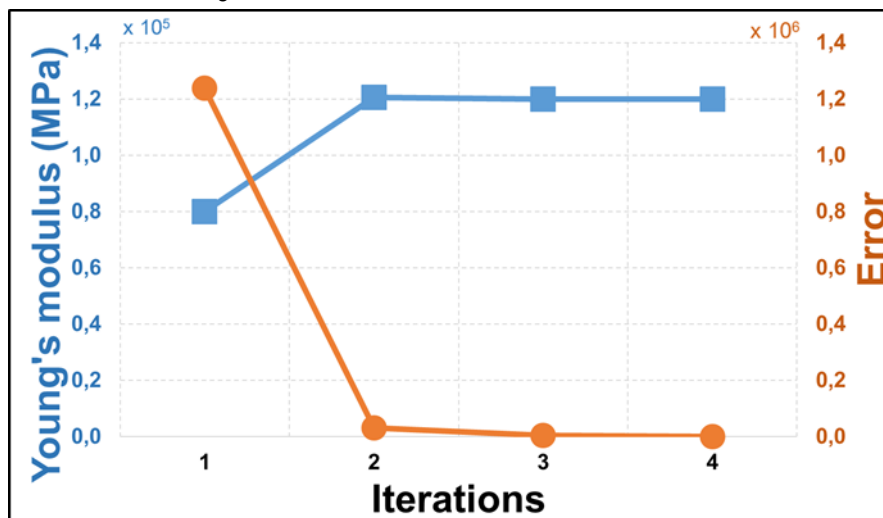


Figure 9: Example of output from the I-DIC algorithm.

4.7. Wedge splitting test at room temperature and elevated temperature

The wedge splitting test is frequently applied for Mode I fracture testing of coarse grained refractories, concrete and wood. It enables stable crack propagation even for relatively large specimen dimensions due to the action of the wedge and the relatively high fracture surface to sample volume relation. Main outcome of the test is the load displacement curve, from which the specific fracture energy G_f and the nominal notch tensile strength σ_{NT} is calculated.

In many cases, a significant fracture process zone is developed during the wedge splitting test. This is especially the case for refractories with reduced brittleness. The observation of the fracture process development is possible for example by DIC (digital image correlation) evaluation of pictures taken during the wedge splitting test.

The wedge splitting test can be carried out under room temperature and elevated temperature (20-1400°C). Additionally the furnace enables gas purging. Figure 10 displays the testing setup, Figure 11: Wedge splitting test sample geometry the sample geometry and Table 3 describes the parts used.

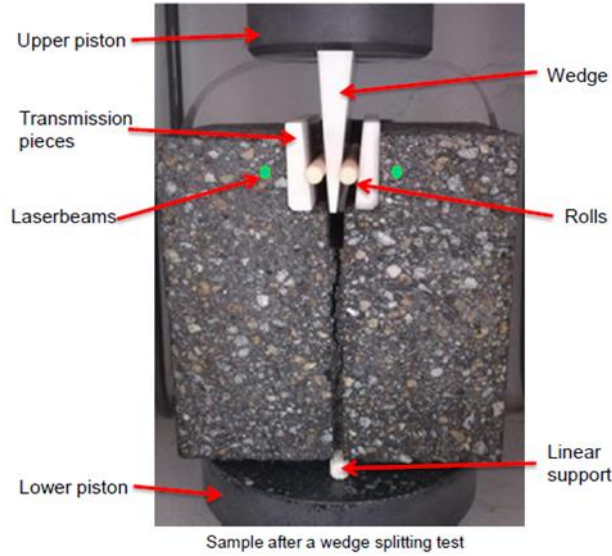


Figure 10: Setup of the wedge splitting test.

Table 3: Parts used in the wedge splitting test.

Part	Description
Load cell	Maximum capacity : 5kN
Linear support	Facilitate the crack initiation
Laser speckle extensometer	Displacement measurement in μm

The outer dimensions of the sample are $100 \times 100 \times 75 \text{mm}^3$. Further details may be seen in Figure 11 [6, 8]. The horizontal displacement is measured directly on the sample surface via laser speckle extensometer [6, 9]. The green points in Figure 10 mark the location for the displacement measurement.

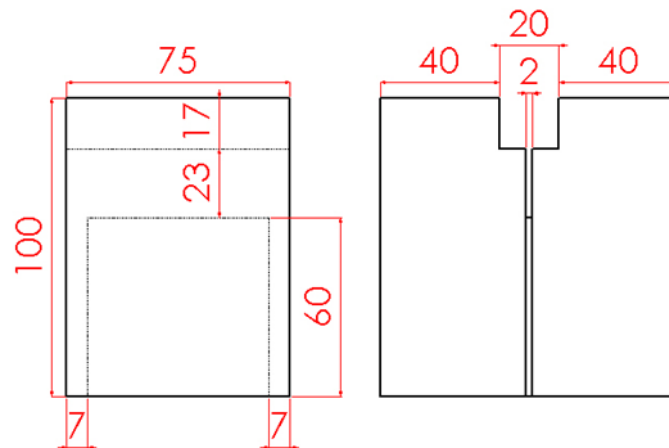


Figure 11: Wedge splitting test sample geometry.

A typical result of a room temperature test is displayed in Figure 12. The figure shows the displacement measured on the front and the rear side and the mean value curve. Usually an abort criterion of 10% of F_{max} is chosen to avoid a collision between wedge and sample. A typical load application rate is 0.5 mm/min.

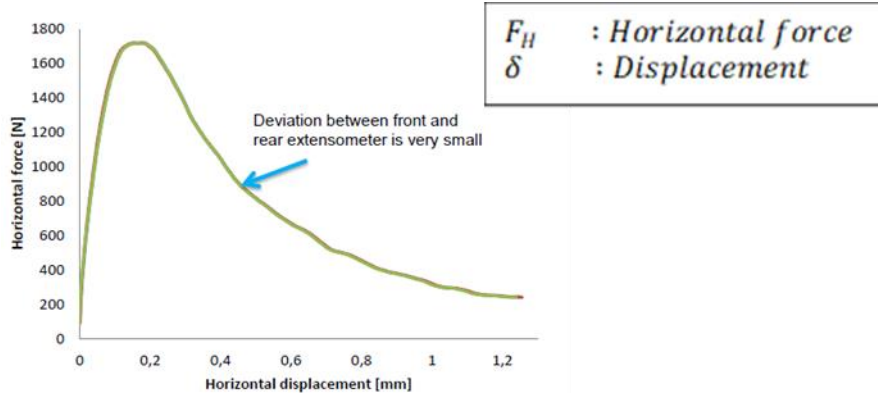


Figure 12: Example of results obtained from the wedge splitting test.

From the raw data obtained, which consist of horizontal force and horizontal displacement, the following parameters can be directly calculated in the following way (Equ. 7, Equ. 8, Equ. 9) [10], [11]:

Specific fracture energy G'_f :

$$G'_f = \frac{1}{A} \int_0^{\delta F_{H,max} 15\%} F_H * d\delta \quad \text{Equ. 7}$$

Notch tensile strength σ_{NT} :

$$\sigma_{NT} = \frac{F_{H,max}}{b * h} * \left(1 + \frac{6 * y}{h}\right) \quad \text{Equ. 8}$$

Characteristic length l_{ch} :

$$l_{ch} = \frac{G'_f * E}{\sigma_{NT}^2} \quad \text{Equ. 9}$$

F_H	: Horizontal force (N)
$F_{H,max}$: Maximum horizontal force(N)
G'_f	: Specific fracture energy ($\frac{N}{m}$)
σ_{NT}	: Notch tensile strength (MPa)
l_{ch}	: Characteristic length (mm)
E	: Young modulus (GPa)
y	: Vertical distance of the horizontal load from the center of gravity of the

The wedge splitting test procedure is well-established for fracture testing of refractories under Mode I conditions. Compared to the bending tests (three point bending, four point bending) and tensile tests the wedge splitting test has several advantages. It allows for stable crack propagation even for relatively brittle materials as well as the formation of a fracture process zone with dimension of up to 50 mm in width and length.

The measurement of the vertical displacement with laser speckle extensometers is more accurate than the displacement from the traverse.

4.8. Mini wedge splitting test device at room temperature

The miniaturized wedge splitting test (WST) device, see Figure 13 and Table 4, allows direct observation of fracture events with light microscope and SEM which is not possible with the standard wedge splitting test out of geometrical reasons. The device will be employed for the identification of fracture mechanism for refractory materials on a microscale level.

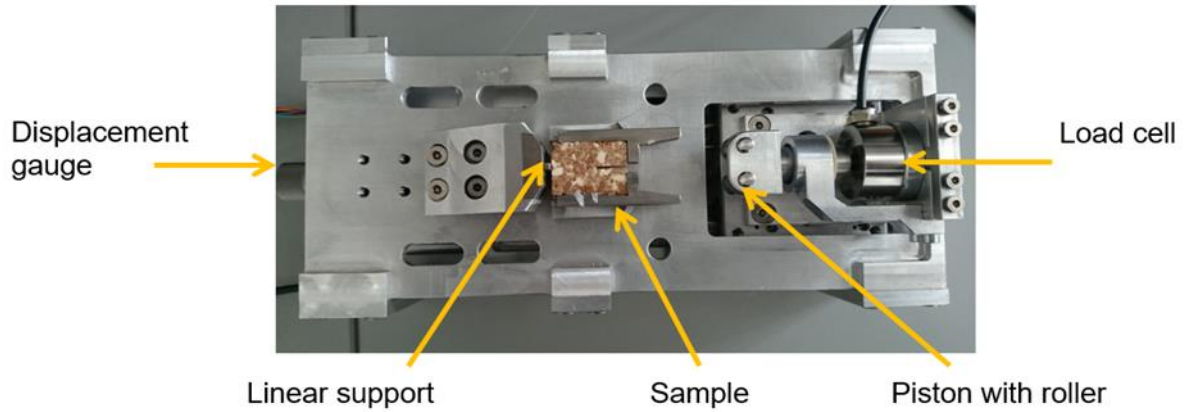


Figure 13: Model of the miniaturised wedge splitting test.

Table 4: Parts used in the Miniaturised wedge splitting test.

Part	Description
Load cell	Maximum capacity: 300N
Piston with roller	Apply the force onto the steel adapters
Linear support	Facilitate the crack initiation
Displacement gauge	Displacement measurement in μm

The miniaturised WST follows the same principle as the standard WST [6]–[8] but using smaller sample geometry ($21 \times 25 \times 8 \text{mm}^3$ detailed with steel adapter Figure 14) compared to the standard geometry ($100 \times 100 \times 75 \text{mm}^3$). The crack propagation will be observed under light microscopy and SEM (Scanning Electron Microscopy). For the application in the SEM the device was designed to work in vacuum conditions. Special lubricants stable under vacuum had to be chosen. As the sample's size of the miniaturised WST is significantly smaller, only the crack initiation can be observed whereas the standard WST allows for pronounced crack branching [12], [13]. Figure 15 shows a typical result obtained from this mini wedge splitting test

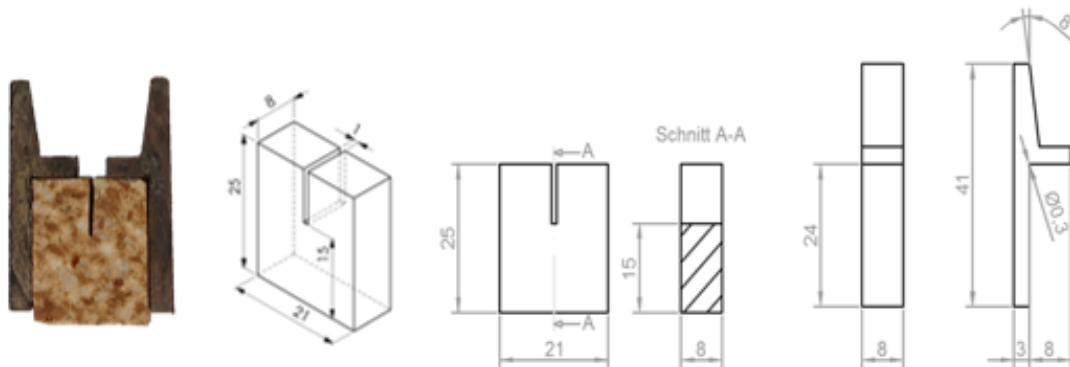


Figure 14: Geometry for a mini wedge splitting test sample and steel adapter.

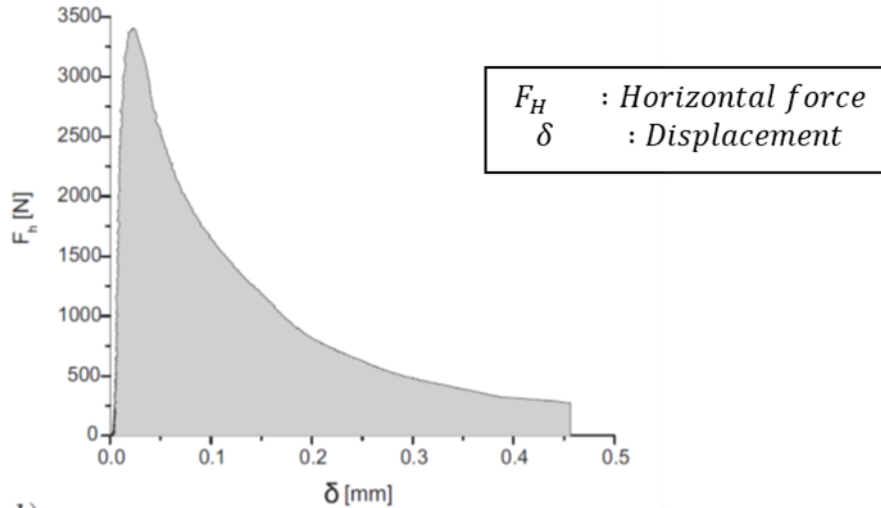


Figure 15: Example for a load / displacement diagram.

From the raw data obtained which consist of horizontal force and horizontal displacement, the following parameters can be directly calculated (Equations Equ. 10, Equ. 11, Equ. 12) [10], [11]:

Specific fracture energy G'_f :

$$G'_f = \frac{1}{A} \int_0^{\delta F_{H,max}^{15\%}} F_H * d\delta \quad \text{Equ. 10}$$

Notch tensile strength σ_{NT} :

$$\sigma_{NT} = \frac{F_{H,max}}{b * h} * \left(1 + \frac{6 * y}{h} \right) \quad \text{Equ. 11}$$

Characteristic length l_{ch} :

$$l_{ch} = \frac{G'_f * E}{\sigma_{NT}^2} \quad \text{Equ. 12}$$

- F_H : Horizontal force (N)
- $F_{H,max}$: Maximum horizontal force(N)
- G'_f : Specific fracture energy ($\frac{N}{m}$)
- σ_{NT} : Notch tensile strength (MPa)
- l_{ch} : Characteristic length (mm)
- E : Young modulus (GPa)
- y : Vertical distance of the horizontal load from the center of gravity of the

The first results are visualised in Figure 16 for magnesia spinel.

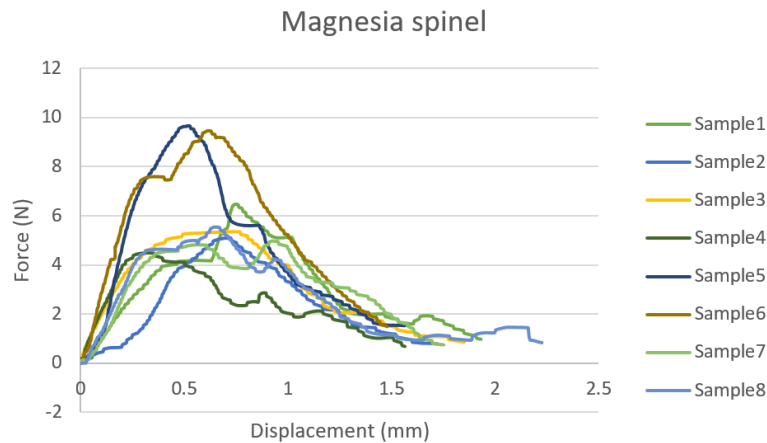


Figure 16: Results from mini WST with magnesia spinel.

4.9. Uniaxial tensile creep test device

The uniaxial tensile creep test allows investigation of creep behaviour in high temperature and under tensile loads. Since there were no standardized methods for describing the high temperature tensile creep behaviour of heavy ceramic refractory materials, the uniaxial tensile creep test has been developed (Figure 17). According to refractory material characteristics, accurate and long term measurements of small displacements at high temperatures (up to 1600°C) with a suitable alignment (to avoid bending), and applying uniform uniaxial stresses, are essential. These factors were considered in the design of the current test apparatus (Table 5) [12], [13].

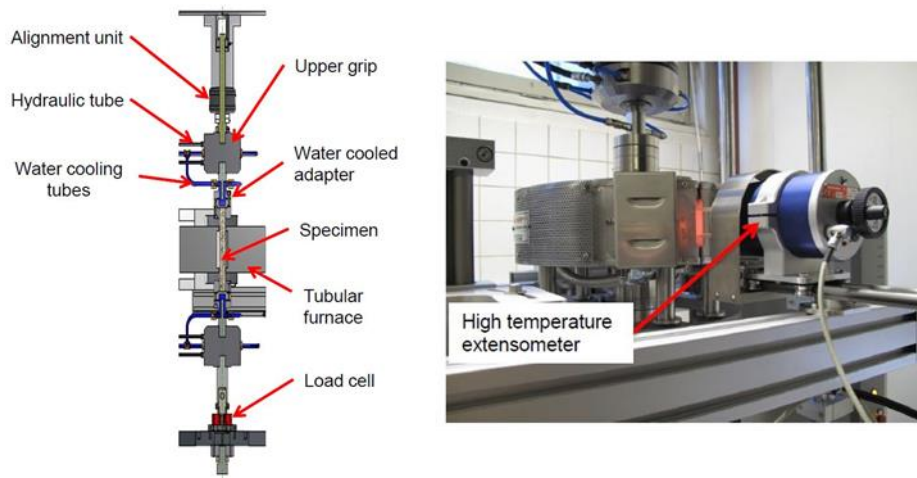


Figure 17: Uniaxial tensile creep testing device.

Table 5: Parts used in the uniaxial tensile creep test device.

Main Parts	Description
Loading parts with load cell	Load up to 20 kN
High temperature tubular furnace	Temperature up to 1700°C
Two mechanical extensometer	Measurement principle: linear variable differential transformer (LVDT)

The design of the specimen shape was completed with help of simulation in order to ensure the viability of the tensile creep measurements. The specimen geometry is a cylinder with 30mm diameter (sufficient due to the size of biggest grains) and 230mm height drilled from bricks; considering that only 100mm of the middle part of the sample is heated by the furnace. Then the sample together with water cooled adapters are aligned and glued onto the fixing device (Figure 18); the fixing device keeps the sample perfectly straight. After the glue hardens, the specimen is introduced in the test machine in vertical orientation. The homogeneity

of temperature in the measured area is assured by placing 3 thermocouples at its surface; and the uniformity of the stress field is also verified by room-temperature measurements using the strain gauges method. The alignment of the machine was certified according to ASTM E1012.

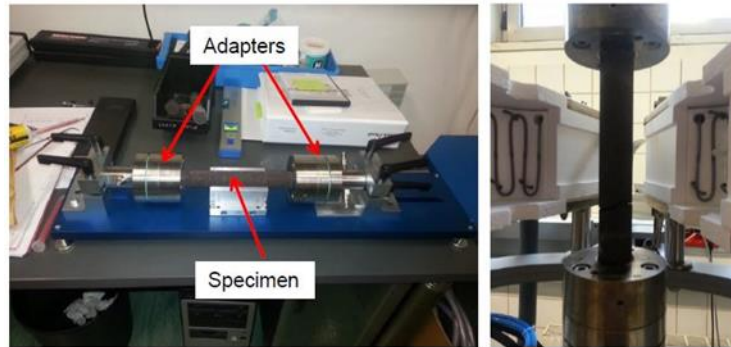


Figure 18: Uniaxial tensile creep test setup and sample.

Heating of the specimen with 5°C/min to testing temperature is the next step; also 1 hour holding time is considered for homogenization of temperature in the specimen. Then the desired load is applied and two extensometers measure the displacement in the surface of the sample (Sensor arm distance: 50 mm). The diagram below shows a typical result of a uniaxial tensile creep test (Figure 19).

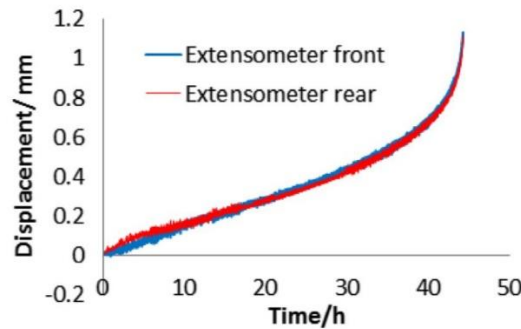


Figure 19: Uniaxial tensile creep test result of a specific sample.

After obtaining strain/time data, these data are employed with an inverse evaluation method in order to determine the creep law parameters. Many models have been suggested to describe the creep behaviour of materials in terms of stress, time and temperature based on uniaxial tests, among which the Norton-Bailey creep law is mostly applied (Equ. 13).

Norton-Bailey law :

$$\dot{\epsilon}_{cr,j} = K_j(T) \times \sigma^{nj} \times \epsilon_{cr}^{aj} \tag{Equ. 13}$$

- j* : creep stage
- n* : stress exponent
- a* : creep strain exponent
- K(T)* : temperature dependant function
- σ :: applied load
- ϵ_{cr} : creep strain

The inverse estimation procedure (Figure 20) is performed separately for each temperature. Also for an accurate inverse estimation of the creep parameters at least three creep curves under different loads are necessary.

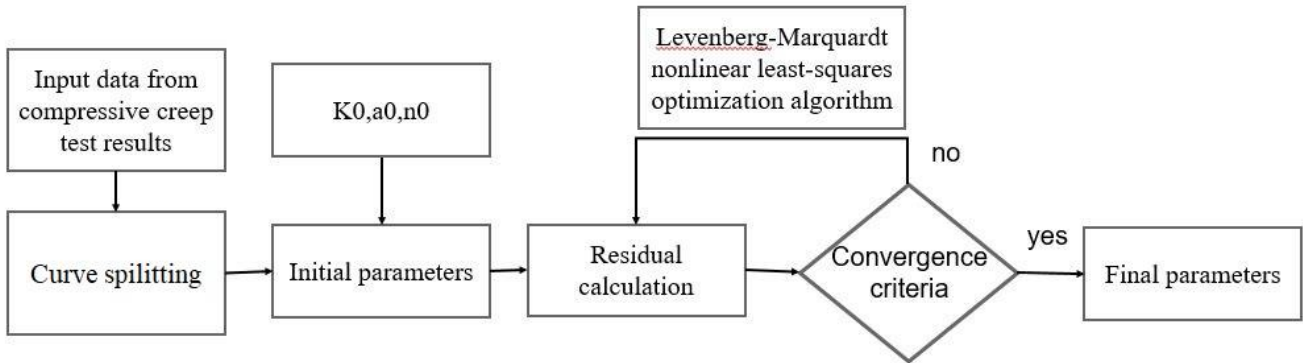


Figure 20: Inverse estimation approach to define the Norton-Baily creep parameters.

Inverse evaluated result's curves obtained for all tensile creep stages of a selected material tested at 1450°C are shown Figure 21.

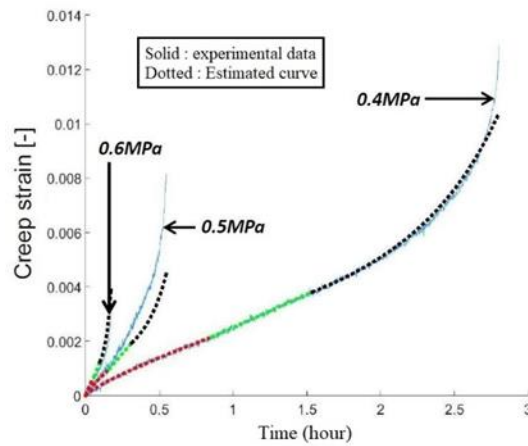


Figure 21: Example of an inverse estimation result of a specific material

4.10. Uniaxial compressive creep test device

The uniaxial compressive creep test allows investigation of creep behaviour at high temperature and under compression. The apparatus (Figure 22, Table 6) was developed to overcome the disadvantages of previous testing approaches like RUL (Refractoriness Under Load) and CIC (Creep In Compression). In contrast to these approaches, higher loads can be applied in the current method (similar to the real world); also the load is applied after reaching the target temperature, so the starting point of creep is well defined [14], [15].

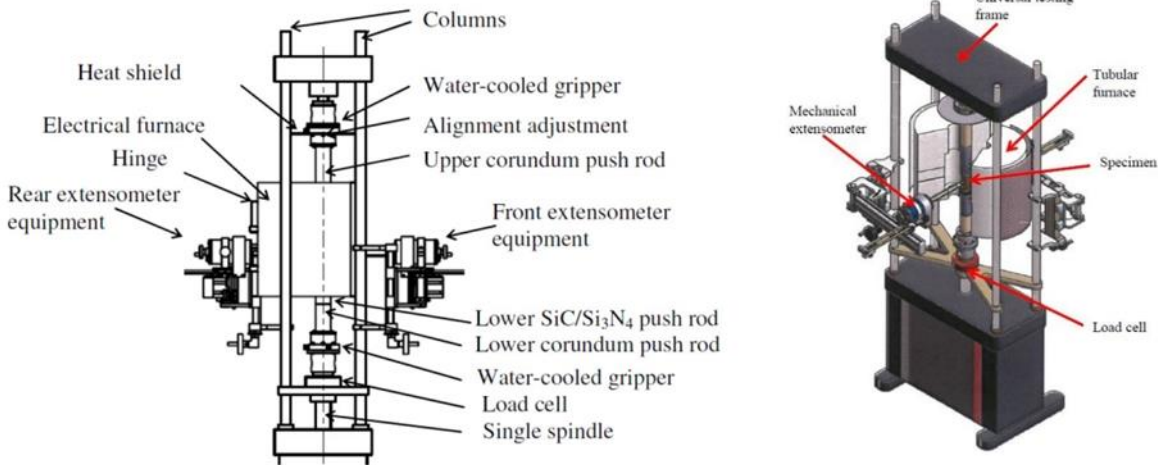


Figure 22: Compressive creep testing device.

Table 6: Parts used in the compressive creep testing device.

Main Parts	Description
Loading parts with load cell	Load up to 10KN at 1400°C
High temperature tubular furnace	Temperature up to 1600°C, heating rate up to 10°C/min
Two mechanical extensometer	Measurement principle: linear variable differential transformer (LVDT)

Preparation of the sample is the first step in the uniaxial compressive creep test procedure. Cylindrical shape specimens with diameter of 35mm and height of 70mm are drilled and inserted in the creep device (Figure 23). Then alignment of the sample is confirmed at room temperature by performing an elastic test and checking the extensometers measurement on both sides of the sample. A height to diameter ratio of 2/1 reduces the impact of friction between the bearing and the specimen in the measured area. In addition, considering an intermediate bearing component constructed of a creep resistant material can homogenize the stress distribution.

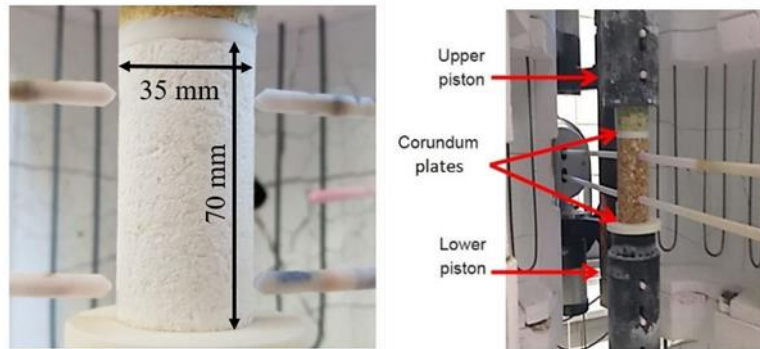


Figure 23: Geometry for uniaxial compressive creep test sample and sample arrangement.

Heating of the specimen with 10°C/min to testing temperature is the next step, also 1 hour holding time is considered for homogenization of temperature in the specimen. Then the desired load is applied and two extensometers measure the displacement in the surface of the sample (Sensor arm distance: 50 mm). The diagram below shows a typical result of a uniaxial compressive creep test (Figure 24).

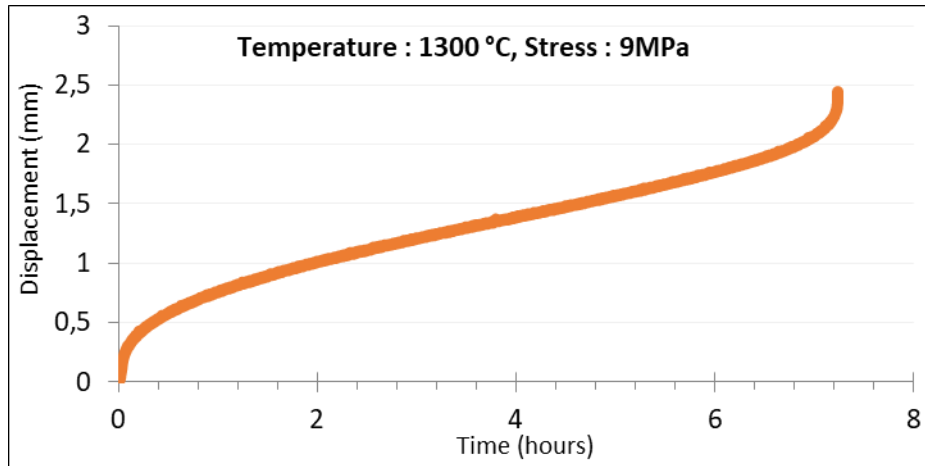


Figure 24: Uniaxial compressive creep test result of a selected sample.

After obtaining strain/time data, an inverse evaluation is applied in order to determine the creep law parameters. Many models have been suggested to describe the creep behaviour of materials in terms of stress, time and temperature based on uniaxial tests, among which the Norton-Bailey creep law is mostly applied (Equ. 14).

Norton-Bailey law :

$$\dot{\epsilon}_{cr,j} = K_j(T) \times \sigma^{nj} \times \epsilon_{cr}^{aj} \tag{Equ. 14}$$

j : creep stage
n : stress exponent
a : creep strain exponent
K(T) : temperature dependant function
 σ :: applied load
 ϵ_{cr} : creep strain

The inverse evaluation procedure (Figure 25) is performed separately for each temperature. For an accurate inverse evaluation of the creep parameters at least three creep curves under different loads are necessary.

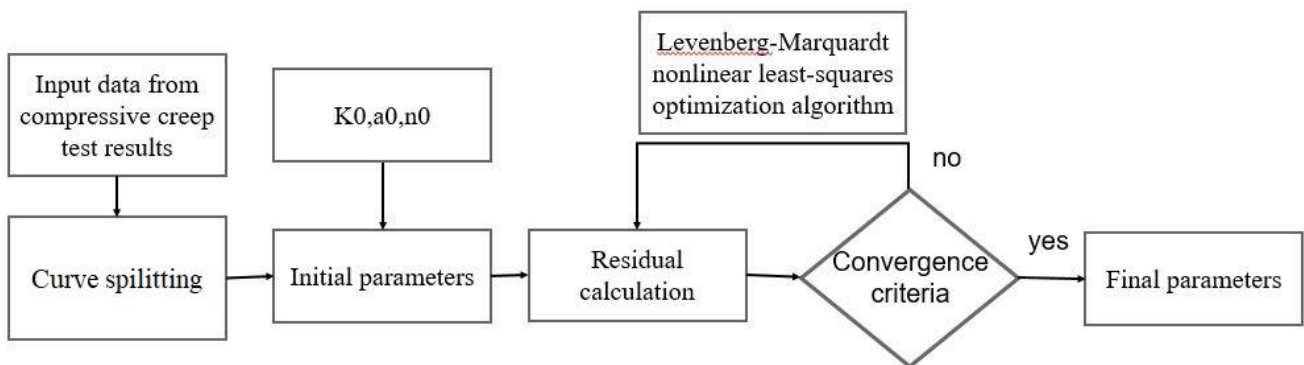


Figure 25: Inverse estimation approach to define the Norton-Bailey creep parameters.

In Figure 26, inverse evaluated result's curves obtained from the first compressive creep stage of a selected material are displayed together with experimental results from 1300°C.

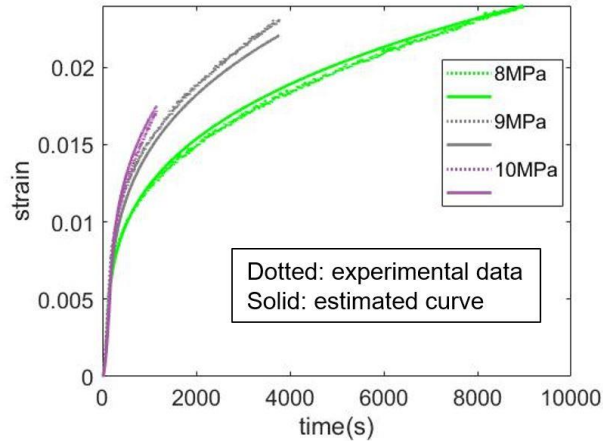


Figure 26: Example of an inverse evaluated result for first creep stage of a selected material.

4.11. RFDA - Resonant Frequency and Damping Analyser

Resonant frequency and damping analyser rely on the impulse excitation technique (IET) to determine a set of fundamental resonant frequencies f_r and for each of them a damping value. Based on the dimensions, mass and resonant frequencies the elastic properties (E , G , ν) are determined.

In the impulse excitation technique the sample is excited by slight mechanical impact in the vibration's anti-node. The vibration nodes depend on sample shape and desired vibration mode. Figure 27 shows an example of nodes configuration for flexural and torsional vibration.

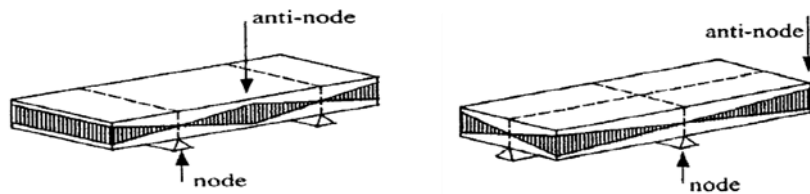


Figure 27: Configuration of nodes and anti-nodes for flexural and torsional vibration.

An acoustic signal is detected by a non-contact transducer (microphone) and recorded in time domain. RFDA software performs a Fast Fourier transformation to determine set of approximate resonant frequency values. The measurement of resonant frequencies allows the determination of elastic properties: Young's modulus, shear modulus and Poisson's ratio. Young's modulus and shear modulus can be calculated from Equ. 15 and Equ. 16 respectively.

$$E = 0.9465 \rho f_r^2 \left(\frac{L^4}{t^2}\right) T_1 \tag{Equ. 15}$$

where f_r - flexural frequency, ρ - density, L - length, t - thickness, T_1 - correction factor ($=f(t/L$ and Poisson's ratio)).

$$G = \frac{4Lmf^2}{bt} \left[\frac{B}{1+A} \right] \tag{Equ. 16}$$

where f_r - torsional frequency

Internal friction, damping or mechanical loss Q^{-1} can be determined for each f_r with the use of RFDA system. To obtain the Q^{-1} value an iterative simulation of the time-domain signal as a sum of exponentially damped sinusoidal functions is conducted. Internal friction Q^{-1} and resonant frequencies f_r are related by the Equ. 17:

$$Q^{-1} = k / (\pi f_r) \tag{Equ. 17}$$

where k - exponential decay parameter of the vibration component of frequency.

Young's modulus and damping measurements can be performed at high temperature with the use of a HT RFDA system (see Figure 28), with suitable equipment modifications.

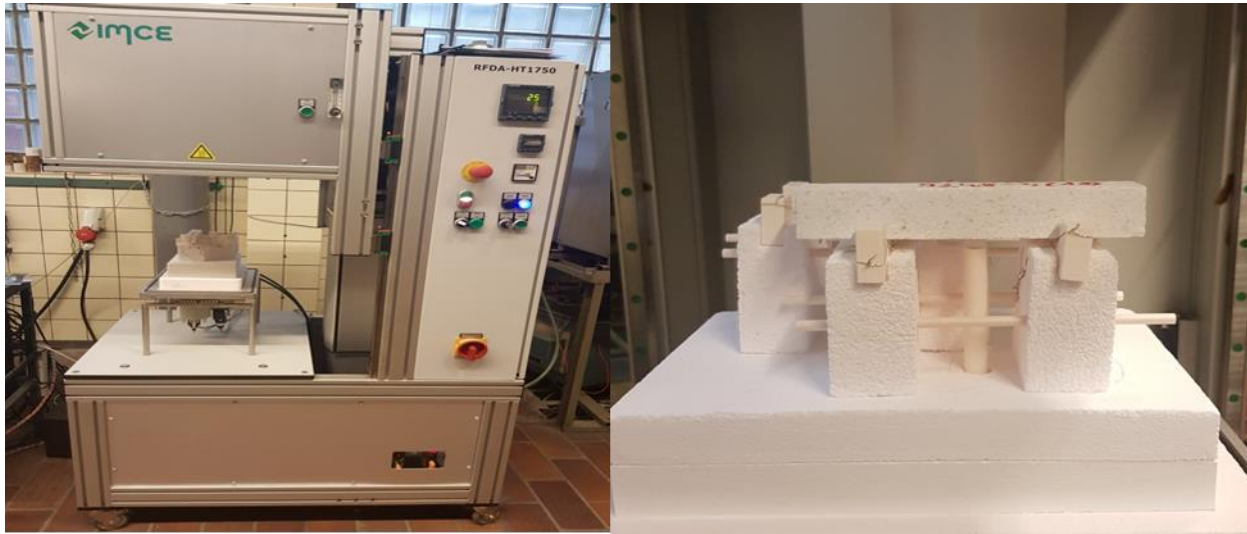


Figure 28: High Temperature RFDA equipment with measurement setup for flexural mode.

Results of Young's modulus and damping temperature dependency obtained with the use of HT RFDA for alumina-spinel brick are visualised in Figure 29.

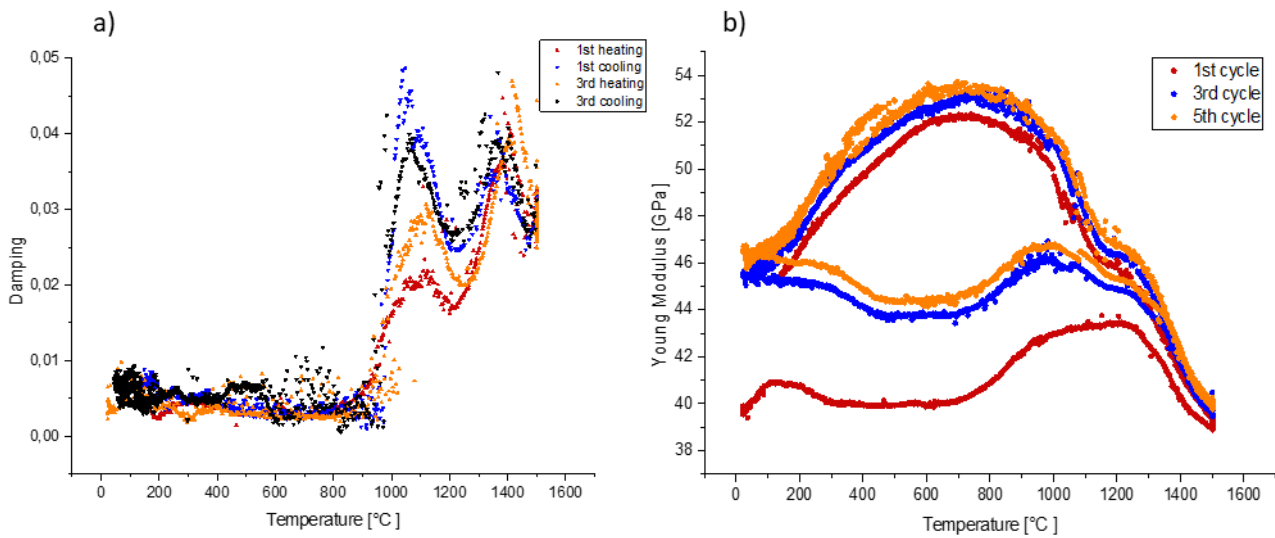


Figure 29: Results obtained with the use of High Temperature RFDA, a) Damping and b) Young's modulus temperature dependency.

4.12. Diametrical compression test (Brazilian test) at room temperature combined with Digital Image Correlation

The Brazilian test is used to investigate the tensile strength of the materials using parts described in Table 7. It could be an index for the overall strength of the materials. As detailed in Figure 30, the experiment is carried out by applying a vertical diametrical compressive force along the thickness of a cylindrical specimen until failure occurs [4]. These specific loading conditions induce horizontal tensile stresses within the specimen and, in some case, could induced relatively high compressive stresses locally in the area close to the contact zone with the jaws. Nevertheless, tensile failure usually occurs rather than compressive failure.

Table 7: Parts used in the Brazilian test.

Part	Description
Loading parts	The supports at IRCER are round, not flat
Load cell	According to the frame of the device, the maximum capacity of Load Cell is 50 kN
DIC Instruments	The strain field at the surface of the sample can be monitored by Digital Image Correlation (DIC)
Strain gauges	Average strain in the central part of the sample can be monitored by strain gauges

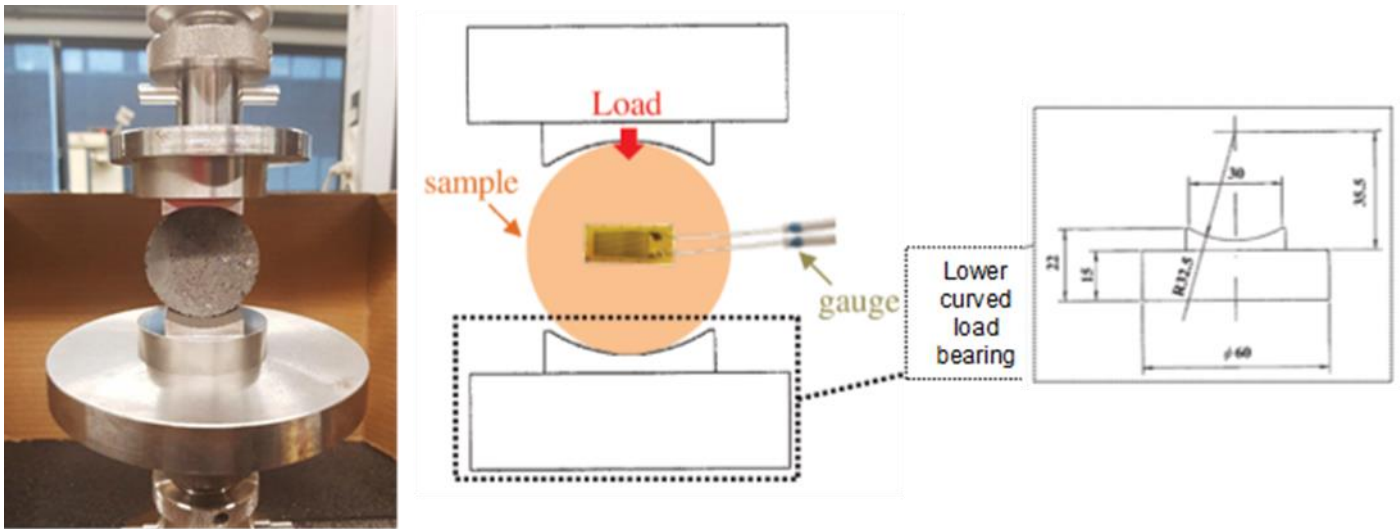


Figure 30: Example of the Brazilian test configuration in IRCER.

The typical output of this test is a force-displacement curve, and in case of using Digital Image Correlation (DIC), it is possible to also obtain strain field evolution versus applied load. This test is easy to handle and is currently used by many communities including refractories. Sample preparation requires specific attention to obtain repeatable results. According to ASTM D3967-95a, the test specimen shall be a circular disk with a thickness-to-diameter ratio (e/D) between 0.2 and 0.75 to be in a plane stress configuration. The diameter of the specimen shall be at least ten times greater than the largest grain within the microstructure of the investigated material. The thickness-to-diameter ratio of 0.2 (the thinnest samples) is used in IRCER. Based on the configuration of the jaws in IRCER (shown in Figure 31), the ratios are suitable to produce a rupture in the centre of the sample [5].

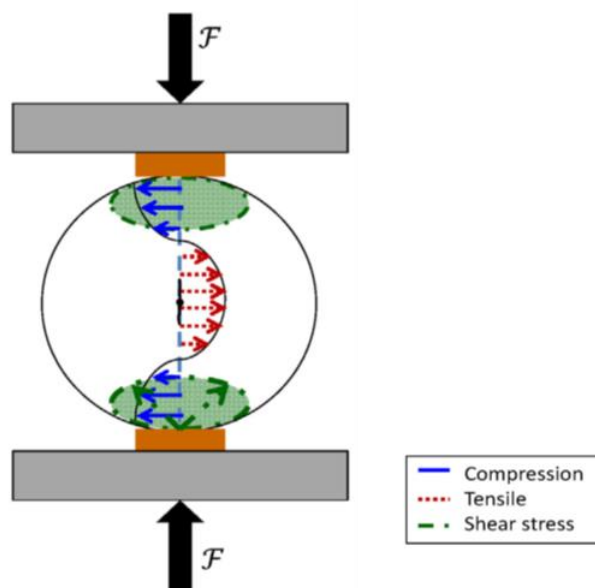


Figure 31: The typical stress distribution in a Brazilian test.

In the Brazilian test, the tensile stress is determined using the following Equ. 18:

$$\sigma_t = \frac{2.P}{\pi.e.D} \quad \text{Equ. 18}$$

where P (N), e (m) and D (m) are the vertical applied load, thickness and diameter of the cylindrical sample respectively.

The primary objective of this test is to determine material tensile strength. Nevertheless, some authors investigated the possibility to characterise elastic properties and fracture parameters [16]–[18].

4.13. DEBEN device for "in situ" room temperature micromechanical test

The micro-platine test device can be used to characterize the thermomechanical properties of refractories at very local scale, in particular with regards to the effect of microstructure of the material. This device (DEBEN Co. MT5000), recently acquired by IRCER, is up to now just operational to manage bending test with very small samples (typically parallelepipeds of 55x10x3 mm). As shown in Figure 32, for such bending test, the sample can be subjected to a 4-point bending force. The parts of this device are detailed in Table 8.

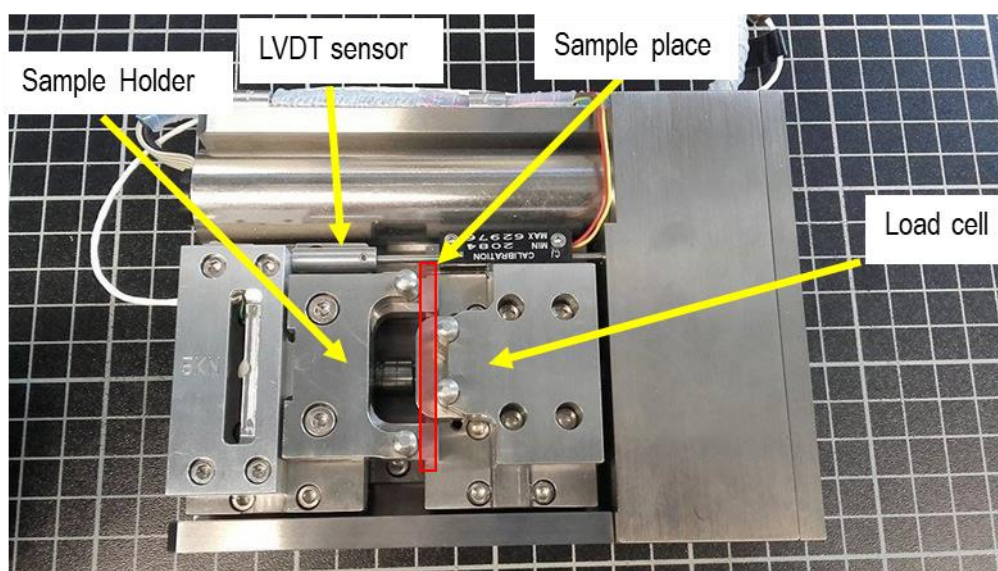


Figure 32: The Micro-Platine test device in the 4-point bending test configuration.

The compactness of the device (approximately 15 centimetres long, 12 centimetres wide and 4 centimetres high) allows to use it under optical microscopy or even within the vacuum chamber of a scanning electronic microscope. This important point allow thus to observe the effects of mechanical stresses on the microstructure of the materials.

Table 8: Parts used in the Micro-Platine test device.

Part	Description
Main characteristics	DEBEN Co. micro-platinum is approximately 15 centimetres long, 12 centimetres wide and 4 centimetres high (weighs 5 kg)
Frame capacity	Maximum capacity: 5 kN
Load cells	Three types of charge cells can be used: 660N, 2000N or 5000N
Speeds of extension	Displacement speed from 0.1 to 1.25 mm/min
LVDT sensor	Can measure displacement between two sample holders
Sample place	It can be configured for 4 different mini tests: uniaxial compression test, direct tensile test, 3-point bending test, 4-point bending test
Sample holder	Fix the sample for DIC treatment
DIC Instruments	Used for monitoring the strain field by Digital Image Correlation (DIC)

4.14. Cyclic Thermal Shock Test - The Twin-chamber equipment

The Twin-chamber equipment [20] allows a cyclic thermal shock to be applied on a refractory specimen in an unconstrained condition between two elevated temperatures in a close system (Figure 33, Table 1). A full cycle consists of one cold shock and one hot shock. In comparison with the tests where thermal cycles are done between one high temperature and the ambient air, tests between two high temperatures allow a more realistic representation of the in-service conditions.

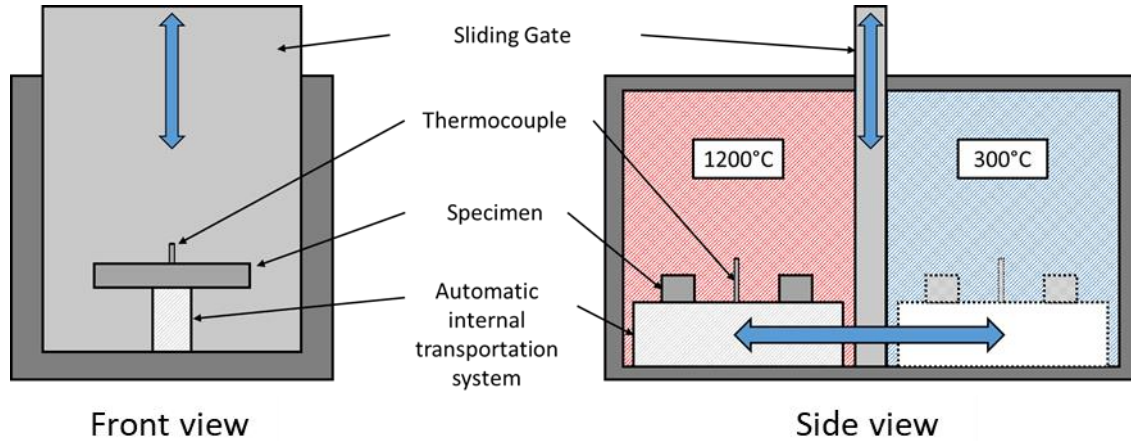


Figure 33: Schematic concept of Twin-chamber equipment and its components.

Table 9: Description of sample movement in the Twin-chamber equipment.

Part	Description
Blue area	Cold chamber
Red area	Hot chamber
Vertical arrow	Moving direction of the sliding gate
Horizontal arrow	Moving direction of the specimen holder

The test is employed for studying the resistance of refractories to repetitive thermal shock loads. According to standards [21], the resistance of a material is determined by the development of crack(s) (Figure 34) as well as the loss of Young's modulus and residual strength (Figure 35) of the specimen after applying thermal cycles [22].

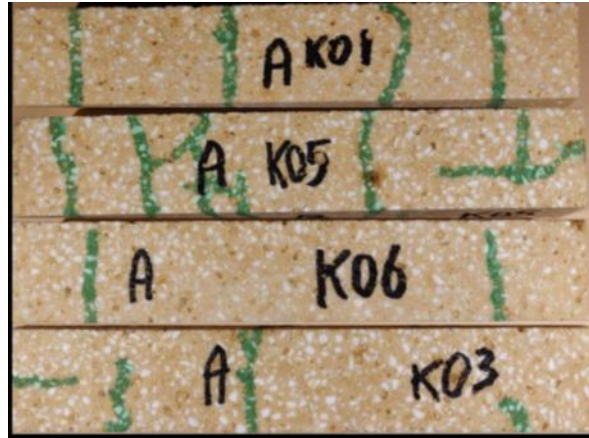


Figure 34: The development of cracks on 4 samples of material SB1 after 50 thermal cycles between 1200°C and 300°C.

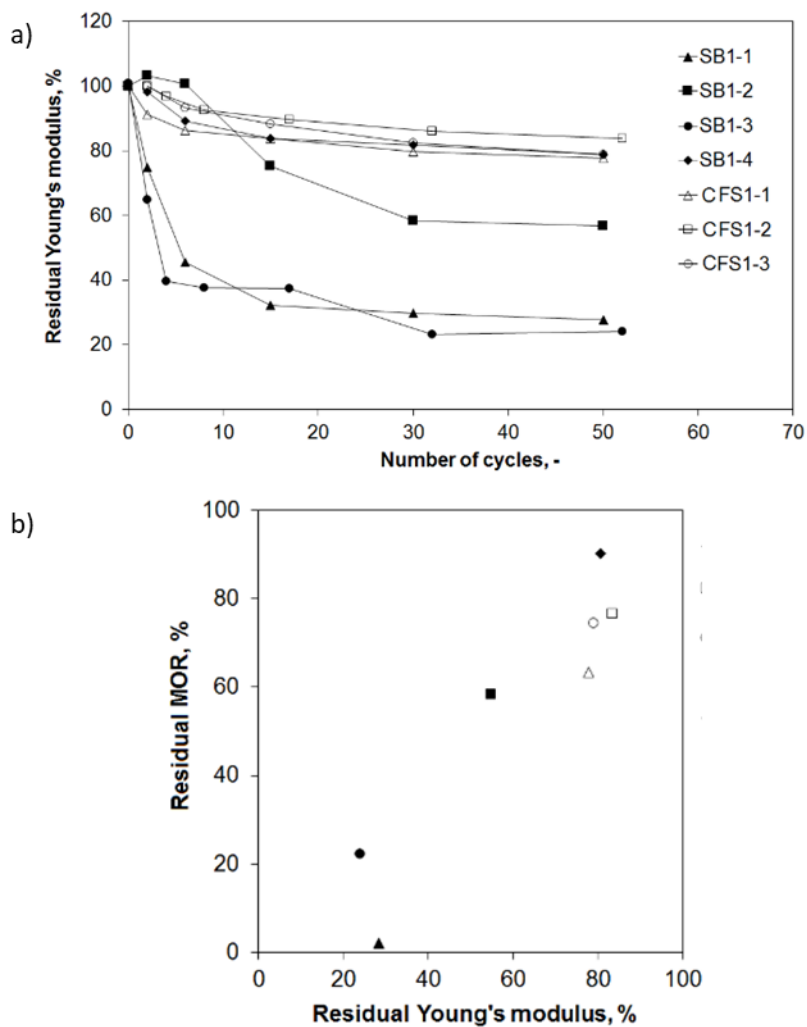


Figure 35: Results of the thermal shock experiments for materials SB1 and CFS1: (a) residual dynamic Young's modulus, (b) correlation of residual dynamic Young's modulus and MOR after 50 thermal cycles in the samples.

5. References

- [1] N. Tessier-Doyen, 'Etude expérimentale et numérique du comportement thermomécanique de matériaux réfractaires modèles', thesis, Limoges, 2003.
- [2] Y. Lalau *et al.*, 'A method for experimental thermo-mechanical aging of materials submitted to concentrated solar irradiation', *Sol. Energy Mater. Sol. Cells*, vol. 192, pp. 161–169, Apr. 2019.
- [3] R. Grasset-Bourdel, 'Structure/property relations of magnesia-spinel refractories: experimental determination and simulation', Thèse de doctorat, Université de Limoges, France, 2011.
- [4] Y. Belrhiti, 'Etude de matériaux réfractaires à comportement mécanique non linéaire par mesure de champs de déformations', Thèse de doctorat, Université de Limoges, France, 2015.
- [5] C. Gazeau, J. Gillibert, E. Blond, P.-M. Geffroy, and N. Richet, 'Experimental set up for the mechanical characterization of plane ITM membrane at high temperature', *J. Eur. Ceram. Soc.*, vol. 14, no. 35, pp. 3853–3861, 2015.
- [6] Y. Dai, D. Gruber, and H. Harmuth, 'Observation and quantification of the fracture process zone for two magnesia refractories with different brittleness', *J. Eur. Ceram. Soc.*, vol. 37, no. 6, pp. 2521–2529, Jun. 2017.
- [7] H. Harmuth, K. Rieder, M. Krobath, and E. Tschegg, 'Investigation of the nonlinear fracture behaviour of ordinary ceramic refractory materials', *Mater. Sci. Eng. A*, vol. 214, no. 1, pp. 53–61, Aug. 1996.
- [8] E. K. Tschegg, K. T. Fendt, Ch. Manhart, and H. Harmuth, 'Uniaxial and biaxial fracture behaviour of refractory materials', *Eng. Fract. Mech.*, vol. 76, no. 14, pp. 2249–2259, Sep. 2009.
- [9] Y. Dai, D. Gruber, and H. Harmuth, 'Determination of the fracture behaviour of MgO-refractories using multi-cycle wedge splitting test and digital image correlation', *J. Eur. Ceram. Soc.*, vol. 37, no. 15, pp. 5035–5043, Dec. 2017.
- [10] H. Harmuth and E. K. Tschegg, 'A Fracture Mechanics Approach for the Development of Refractory Materials with Reduced Brittleness', *Fatigue Fract. Eng. Mater. Struct.*, vol. 20, no. 11, pp. 1585–1603, 1997.
- [11] H. Harmuth and R. Bradt, 'Investigation of Refractory Brittleness by Fracture Mechanical and Fractographic Methods | Fracture | Fracture Mechanics', in *Refractories manual*, 2010.
- [12] A. Sidi Mammam, D. Gruber, H. Harmuth, and S. Jin, 'Tensile creep measurements of ordinary ceramic refractories at service related loads including setup, creep law, testing and evaluation procedures', *Ceram. Int.*, vol. 42, no. 6, pp. 6791–6799, May 2016.
- [13] A. S. Mammam, 'Investigation of High Temperature Tensile Creep of Refractories', University of Leoben, 2016.
- [14] S. Jin, H. Harmuth, and D. Gruber, 'Compressive creep testing of refractories at elevated loads—Device, material law and evaluation techniques', *J. Eur. Ceram. Soc.*, vol. 34, no. 15, pp. 4037–4042, Dec. 2014.
- [15] S. Jin, 'Investigation of compressive refractory creep', University of Leoben, 2015.
- [16] D. Li and L. N. Y. Wong, 'The Brazilian Disc Test for Rock Mechanics Applications: Review and New Insights', *Rock Mech. Rock Eng.*, vol. 46, pp. 269–287, Mar. 2013.
- [17] T. Akazawa, 'New test method for evaluating internal stress due to compression of concrete: the splitting tension test', *Jpn. Soc. Civ. Eng.*, vol. 29, pp. 777–787, 1943.
- [18] G. E. Andreev, 'A review of the Brazilian test for rock tensile strength determination. Part I: calculation formula', *Min. Sci. Technol.*, vol. 13, no. 3, pp. 445–456, Dec. 1991.
- [19] DEBN, 'DEBN : Microscope accessory solutions - In-situ Tensile Stages, microtest overview'.
- [20] J. Schnieder *et al.*, 'Fracture process zone in refractory castables after high temperature thermal shock', *Refract World Forum*, vol. 8, pp. 74–80, 2016.
- [21] 'Methods of test for dense shaped refractory products - Part 11: Determination of resistance to thermal shock; German version EN 993-11:2007', Beuth Verlag GmbH.
- [22] K. Andreev, V. Tadaion, Q. Zhu, W. Wang, Y. Yin, and T. Tonnesen, 'Thermal and mechanical cyclic tests and fracture mechanics parameters as indicators of thermal shock resistance: case study on silica refractories', *J. Eur. Ceram. Soc.*, 2019.